Cancer Immunology, Immunotherapy (2025) 74:183
https://doi.org/10.1007/s00262-025-04042-y

RESEARCH

Blockade of TIGAR prevents CD8$^+$ T cell dysfunction and elicits anti-AML immunity

Jialin Cui[1] · Wenjie Liu[2] · Shiyang Zhong[3,4] · Yiran Fang[2] · Pei Xu[2] · Cheng Xu[5] · Rong Wang[2] · Xingfei Hu[3,4] · Wanting Zhou[3,4] · Kening Li[3,4] · Ming Hong[2] · Sixuan Qian[2] · Qian Sun[2]

Received: 2 September 2024 / Accepted: 1 April 2025

Abstract

Acute myeloid leukemia (AML) cells and activated T cells rely on aerobic glycolysis for energy metabolism. The TP53-induced glycolysis and apoptosis regulator (TIGAR) inhibits glycolysis and protects AML cells from apoptosis. Preliminary studies suggest that combining TIGAR inhibition with the glycolysis inhibitor 2-deoxy-D-glucose (2-DG) may offer a therapeutic strategy for AML. However, it remains unclear whether silencing TIGAR can enhance T cell function and thereby improve AML prognosis. This study aims to investigate whether TIGAR silencing in host can eliminate AML cells and rejuvenate dysfunctional T cells with mouse models. TIGAR knockout mice on the C57BL/6J background were generated and AML mouse models were established through intravenous injection of C1498 cells. We found that TIGAR depletion enhanced CD8$^+$ T cell counts and raised CD4/CD8 ratio, downregulating CD44 and immune checkpoints CTLA-4, LAG-3, PD-1 on cell surface of CD8$^+$ T cells. TIGAR depletion boosted cytokine secretion (IFN-γ, perforin, granzyme B, TNF-α) by CD8$^+$ T cells and IL-2, TNF-α by CD4$^+$ T cells, improving cytotoxicity against AML cells, proliferation, and reducing apoptosis. TIGAR suppression in host with 2-DG prolonged AML mouse survival, decreased tumor burden, and leukemic infiltration. TIGAR suppression restored thymic T cell development and peripheral immune balance. Single-cell RNA sequencing analysis also revealed that high TIGAR expression influences the glycolysis pathway, and correlates with markers of T cell exhaustion. This study indicates that blocking TIGAR prevents CD8$^+$ T cell dysfunction and induces anti-AML immunity.

Keywords Acute myeloid leukemia · Knockout mice · T-lymphocytes · TP53-induced glycolysis and apoptosis regulator · Single-cell RNA sequencing

Abbreviations

2-DG	2-deoxy-D-glucose
AML	Acute myeloid leukemia
ATP	Adenosine triphosphate
BP	Biological processes
CC	Cellular components
CFSE	Carboxyfluorescein succinimidyl este
CTLA-4	Cytotoxic T-lymphocyte-associated protein 4
DMEM	Dulbecco's modified eagle medium
DN	Double negative
DP	Double positive
EdU	5-ethynyl-2′-deoxyuridine
ELISA	Enzyme-linked immunosorbent assay

Jialin Cui, Wenjie Liu, Shiyang Zhong have contributed equally to this work and share first authorship.

✉ Sixuan Qian
qiansx@medmail.com.cn

✉ Qian Sun
kssq001@163.com

[1] Department of Rehabilitation Medicine, The First Affiliated Hospital of Nanjing Medical University, Jiangsu Province Hospital, Nanjing, China

[2] Department of Hematology, The First Affiliated Hospital of Nanjing Medical University, Jiangsu Province Hospital, Nanjing, China

[3] Department of Bioinformatics, Nanjing Medical University, Nanjing, China

[4] Department of Hematology, The Affiliated Huaian No.1 People's Hospital of Nanjing Medical University, Northern Jiangsu Institute of Clinical Medicine, Huaian, China

[5] Department of Pathology, The First Affiliated Hospital of Nanjing Medical University, Jiangsu Province Hospital, Nanjing, China

Published online: 26 April 2025

FBS	Fetal bovine serum
GFP	Green fluorescent protein
GO	Gene ontology
GSEA	Gene set enrichment analysis
H&E	Hematoxylin–eosin
IFN-γ	γ interferon
IQR	Interquartile range
KEGG	Kyoto encyclopedia of genes and genomes
KO	Knockout
LAG-3	Lymphocyte-activation gene 3
MDSCs	Myeloid-derived suppressor cells
MF	Molecular functions
MHC	Major histocompatibility complex
MOI	Multiplicity of infection
NADPH	Nicotinamide adenine dinucleotide phosphate
OXPHOS	Oxidative phosphorylation
PD-1	Programmed cell death protein 1
PD-L1	Programmed death-ligand 1
PD-L2	Programmed death-ligand 2
PFKFB	6-Phosphofructose kinase/fructose-2,6-bisphosphatase
PI	Proliferation index
PI	Propidium iodide
PPP	Pentose phosphate pathway
ROS	Reactive oxygen species
R/R	Relapsed/refractory
scRNA-seq	Single-cell RNA sequencing
SD	Standard deviation
SP	Single positive
ssGSEA	Single sample gene set enrichment analysis
TCR	T cell receptor
TIGAR	TP53-induced glycolysis and apoptosis regulator
TIGIT	T cell immunoglobulin and ITIM domain
TIM-3	T cell immunoglobulin and mucin domain-containing protein 3
TNF-α	Tumor necrosis factor α
Tregs	Regulatory T cells

Introduction

Acute myeloid leukemia (AML) presents challenges due to its complex pathogenesis and genetic diversity [1]. Effective management involves a multifaceted treatment approach integrating targeted therapies with other interventions, acknowledging the disease's multifactorial nature. Recent studies have identified metabolic reprogramming in tumor cells [2, 3], notably aerobic glycolysis or the "Warburg effect," [4] where cells favor glycolysis over mitochondrial oxidative phosphorylation (OXPHOS) for energy production. This metabolic shift supports rapid proliferation by providing adenosine triphosphate (ATP) and raw materials for cell growth [5]. Metabolic changes in tumors are tightly linked to molecular alterations affecting malignancy and prognosis [3, 6, 7]. Our previous reports have also confirmed that AML cells exhibit similar metabolic behaviors, relying on glycolysis for energy [8, 9]. Inhibiting glycolysis can induce apoptosis, pointing to potential targeted therapy opportunities. The competition for energy resources between tumor cells and T cells, switching to glycolysis upon activation, leads to immune suppression and facilitates tumor growth [10–12]. Addressing these dynamics is crucial for combating AML effectively.

TP53-induced glycolysis and apoptosis regulator (*TIGAR*) is a downstream target gene of p53, acting as a 6-phosphofructose kinase/fructose-2,6-bisphosphatase (PFKFB) enzyme to inhibit glycolysis by hydrolyzing fructose phosphates [13]. This inhibition redirects metabolism towards the pentose phosphate pathway (PPP), producing Nicotinamide adenine dinucleotide phosphate (NADPH) and ribose essential for DNA repair and reducing Reactive oxygen species (ROS) levels. TIGAR influences energy balance, autophagy, stem cell differentiation, and cell survival [13–15]. We have previously reported that high TIGAR expression in leukemia cells predicts poor AML outcomes [8, 9, 16]. Silencing TIGAR inhibited the proliferation of human leukemia cells and sensitized leukemia cells to glycolysis inhibitor 2-deoxy-D-glucose (2-DG) both in vitro and in vivo. Furthermore, TIGAR knockdown in combination with 2-DG led leukemia cells to apoptosis [8]. Our preliminary research provides a theoretical basis for the combined treatment of AML with TIGAR inhibition and the glycolysis inhibitor 2-DG. However, it is still unknown whether silencing TIGAR in host with AML can enhance T cell function and thereby improve the prognosis of AML. This study focuses on understanding how TIGAR silencing affects T cell count and function in the setting of AML. We aim to elucidate these mechanisms by using TIGAR knockout (KO) mice with AML and single-cell RNA sequencing (scRNA-seq) to explore novel targets for AML treatment.

Materials and methods

Cell culture

Murine AML cells C1498 (Cell Bank of the Chinese Academy of Sciences, Shanghai, China) were cultured in RPMI 1640 medium containing 10% fetal bovine serum (FBS) (Gibco, USA) and 1% penicillin–streptomycin (Beyotime Biotechnology, China) at 37 °C in a 5% CO_2 humidified incubator. HEK-293 T cells were cultured in Dulbecco's Modified Eagle Medium (DMEM) containing 10% FBS, including L-Glutamine, penicillin, and streptomycin.

Mice and model

Adult (6–8 weeks, weighing 20–25 g) male C57BL/6J mice were provided by Ensiweier Biotechnology Co., Ltd. (Chongqing, China). B6/JNju-Tigarem10Cd8164/Gpt gene mice (TIGAR deficient/TIGAR KO mice on the C57BL/6J background) were provided by Western Biomedical Technology (Chongqing, China). Identification report indicates no statistical difference in various blood routine indexes and percentage of splenic lymphocyte subsets between TIGAR KO and TIGAR WT mice (Supplementary file 1). Approximately 10^6 C1498-GFP (green fluorescent protein) cells (100 µl) were injected into tail veins of C57BL/6J mice and TIGAR KO mice to construct TIGAR WT mice with AML and TIGAR KO mice with AML models, while equal volume of normal saline was injected to construct wild-type control mice. Three to four weeks after cell injection, the experimental mice were euthanized by barbiturate overdose, and the fresh spleen was removed immediately by opening the abdomen for subsequent experiments. The thymus was removed under sterile conditions, and surrounding connective tissue was removed, followed by washing with PBS three times. The thymus was then cut into small pieces and ground on a filter mesh to create a cell suspension, which was resuspended in PBS. Centrifugation was performed, followed by red blood cell lysis. The cell pellet was resuspended in PBS, and CD4/FITC and CD8/APC flow cytometry antibodies were added for incubation, followed by subsequent experiments. In the in vivo experiments, another two groups of mice were also established: one group with 2-DG-treated TIGAR WT mice with AML and the other with 2-DG-treated TIGAR KO mice with AML. These mice were orally administered 2-DG solution at a dose of 2 g/kg once daily from day 1 to day 30. Control groups received an equal volume of saline solution under the same conditions.

Packaging, purification, and transduction of lentiviral vectors

Three lentiviral plasmids (shuttle plasmid LV5, psPAX2, and pMD2.G) were used to make the virus (Gene Pharma, Shanghai, China). The shuttle plasmid carried marker genes which express GFP and resistance genes, and the psPAX2 and pMD2.G plasmids carried components required for virus packaging. GFP-positive cells were used for the construction of mouse models when detecting the quantity of AML in mouse peripheral blood, and fluorescence could be directly measured from peripheral blood to determine the number of AML cells. HEK-293 T cell was used as a host for virus packaging. E. coli strain DH5α was used to amplify lentiviral vectors and help packaging vector plasmids.

HEK-293 T cells ($2–3 \times 10^6$) were seeded in a culture dish with 10 mL of complete medium and incubated overnight. When cells reached 50–70% confluence, the medium was replaced with 10 mL of transduction medium (high-glucose DMEM + 5% FBS) 1–2 h before transduction. Packaging plasmids were diluted in Opti-MEM (tube 1), and NDE3000 reagent (Western Biomedical Technology, Chongqing, China) was diluted in Opti-MEM (tube 2). After mixing, the transduction mixture was incubated at room temperature for 15 min, then gently pipetted and added to the cells, which were returned to the incubator. On day 3, the medium was replaced with fresh complete medium, and cells were cultured for 48 h. On day 5, viral supernatant was collected, transferred to a 50 mL centrifuge tube, and stored at 4 °C. An additional 10 mL of complete medium was added to the dish and incubated overnight. On day 6, the supernatant from day 5 and the additional 10 mL were combined, centrifuged at $5000 \times g$ for 5 min, and filtered through a 0.45 µm syringe filter to remove debris.

Lentiviral titration

Approximately 3×10^4 HEK-293 T cells were seeded per well in 96-well plates and added 100 µl of soup containing different concentrations of virus to each cell. The medium was changed 24 h after transduction and the GFP expression in cells were analyzed using flow cytometry at 72 h post-transduction. The viral titration was 4×10^8 TU/mL.

C1498 cell transduction

C1498 cells were transduced using produced virus particles at the multiplicity of infection (MOI) of 40 in the presence of 5 µg/mL polybrene. After lentiviral transduction and puromycin selection (6 µg/mL), transduction efficiency was evaluated by analysis of GFP expression. The screening was continued for 1 month until the fluorescence rate reached close to 100%, and cells stably expressing GFP (C1498-GFP) were obtained, cultured in bulk expansion, and the fluorescence rate was identified using flow cytometry.

Splenic naïve $CD4^+$ T and $CD8^+$ T cell isolation

Splenic lymphocytes were isolated by Mouse Splenic Lymphocyte Isolation Kit (TBD, Tianjin, China) according to the manufacturer's instructions. Mice naïve $CD4^+$ T or $CD8^+$ T cells were prepared by magnetic beads with Naïve $CD4^+$ T Cell Isolation Kit, mouse (Miltenyi, USA) and Naïve $CD8^+$ ($CD8a^+$) T Cell Isolation Kit, mouse (Miltenyi, USA). The cells were resuspended with RPMI 1640 medium, and the cell density was adjusted to 1×10^6/mL.

Activation of $CD4^+$ and $CD8^+$ T cells

The activation of mouse naïve $CD4^+$ T and $CD8^+$ T cells were induced by encapsulated anti-mouse CD3 antibody (eBioscience, USA) (10 μg/mL) and anti-mouse CD28 antibody (eBioscience, USA) (2 μg/mL), added to the medium containing 20 ng/mL IL-2 (Proteintech, USA) and continued to incubate for 0 h, 12 h, 24 h, 48 h, and 72 h.

Flow cytometry

For surface staining, the monoclonal antibodies listed were used: CD3 (17A2)-FITC, CD4 (GK1.5)-PE, CD4 (GK1.5)-APC, CD8 alpha (5H10)-APC, CD44 (IM7)-FITC, PD-1 (J43)-FITC, CTLA-4 (1B8)-FITC, LAG-3 (C9B7W)-FITC and CD62L (MEL-14)-PE (all from eBioscience, USA). Flow cytometry was done by C6 or FACSVantage SE (both BD Bioscience, USA) for cell analysis.

CCK8 cytotoxicity assays

After isolation and washing with PBS thrice, 100 μl of $CD8^+$ T cells from TIGAR WT mice with AML and TIGAR KO mice with AML were seeded at a concentration of 1×10^5 cells/mL in a 96-well plate. These T cells were mixed with 100 μl of C1498 cells at different effector to target ratios. After incubation for 72 h, 10 μl of CCK-8 solution (Sigma, USA) was added to each well, and the plate was further incubated for 1–4 h. The OD value was measured at 450 nm with an ELISA reader (ThermoFisher, USA). The killing rate of $CD8^+$ T cells on AML cells was calculated using the following formula. AML cell killing rate (%) = $[(OD_E + OD_T)\text{-}OD_{E+T}]/OD_T \times 100\%$. OD_{E+T} represents the OD value of the effectors and targets, OD_E represents the OD value of the effectors alone at the corresponding concentrations, and OD_T represents the OD value of the targets alone at the corresponding concentrations.

Cell proliferation assay

In vitro, $CD8^+$ T cells were obtained and resuspended in PBS, and the cell density was adjusted to 1×10^6/mL. 10 μM carboxyfluorescein succinimidyl este (CFSE) stock solution (eBioscience, USA) was added and incubated at 37 °C for 10 min. Five-fold volume of cold complete culture medium was added to terminate the staining and incubated on ice for 5 min. After being washed three times with fresh culture medium, the cells were centrifuged, resuspended and reseeded into a 6-well plate. The cells were incubated in a 5% CO_2 constant temperature incubator at 37 °C for 72 h, collected, and detected using flow cytometry with excitation light at 488 nm. Proliferation Index (PI) = Total cell count (the sum of the number of cells across all generations)/the number of undivided cells.

In vivo, the C1498-GFP cells were injected via the tail vein into different mouse models, and after 7, 14, and 21 days, 0.1 mg/kg of 5-ethynyl-2′-deoxyuridine (EdU) (Beyotime Biotechnology, China) was intraperitoneally injected 4 h prior to tissue collection. The mice were sacrificed, and the fresh spleens were immediately dissected by laparotomy for subsequent experiments, including splenic lymphocyte isolation. Cell proliferation of $CD4^+$ T and $CD8^+$ T cells at different time point was detected using flow cytometry (FACSVantage SE, BD, USA) with BeyoClick™ EdU-555 cell proliferation detection kit (Beyotime Biotechnology, China).

Cell apoptosis assay

$CD8^+$ T cells from each group were collected and suspended in a 1.5 mL EP tube, followed by centrifugation at 1000 g for 5 min. The supernatant was discarded, and the cells were gently resuspended with 190 μl Annexin V-FITC binding solution (annexin V-Alexa Fluor 647/PI apoptosis detection kit, Invitrogen, USA). Afterwards, 5 μl of Annexin V-FITC and 5 μl of propidium iodide (PI) staining solution were added to the cells, mixed gently, and incubated at room temperature in the dark for 10 min. Flow cytometry was then performed to detect Annexin V-FITC (green fluorescence) and PI (red fluorescence).

Counting of AML cells

To count AML cells in peripheral blood of mice, peripheral blood was collected from mice via enucleation of the eyeball. Blood samples were diluted 1:10 with PBS, centrifuged to isolate cells, and resuspended in PBS at a concentration of 1×10^7 cells/mL. GFP-expressing C1498 cells were analyzed using a flow cytometer with a 488 nm laser. Emitted green fluorescence was detected and converted into electrical signals, which were used to identify and count GFP-positive cells through specific gating. Data were then processed and presented graphically and in tabular formats. Peripheral blood AML cell ratio = Number of GFP-positive C1498 cells/Total blood cell count.

Hematoxylin–eosin (H&E) staining

Spleens and livers of each group of mice were fixed in 4% polyformaldehyde solution and subsequently embedded in paraffin. After embedding, sections of 5-μm thickness were obtained and subsequently stained using standard hematoxylin (Jiancheng Bioengineering Institute, Nanjing, China) and eosin (Biyuntian Biotechnology Co. Ltd. Shanghai, China) staining. Digital images were obtained using an inverted

microscope and camera system (Leica, Germany) following the manufacturer's instructions. Microscopic examination was conducted by two pathologists blinded to group assignments to quantify leukemia infiltration. This was achieved by assessing parameters including the number and distribution of leukemic cells, the disruption of normal tissue architecture, and the extent of tissue infiltration. The pathologists visually identified the areas infiltrated by leukemic cells within the liver and spleen tissues. Using a standardized counting method, the pathologists counted the number of leukemia-infiltrated areas and total area of the liver or spleen tissue section, respectively. The percentage of leukemia in the liver or spleen was calculated as (area of leukemia-infiltrated regions/total area of the tissue section) × 100%. Single-factor ANOVA analysis and the LSD method (Least Squares Difference) were used to compare the differences in the proportion of leukemia cells among the groups.

Enzyme-linked immunosorbent assay (ELISA)

In the in vitro experiments, supernatants of activated $CD8^+$ and $CD4^+$ T cells were collected after freeze–thaw and centrifugation. The levels of γ interferon (IFN-γ), perforin, granzyme B, and Tumor necrosis factor α (TNF-α) in $CD8^+$ T cells, and IL-2 and TNF-α in $CD4^+$ T cells were measured using ELISA kits (Lkcxtech, Beijing, China; MULTI SCIENCES, Beijing, China). In the in vivo experiments, serum concentrations of IFN-γ, perforin, granzyme B, TNF-α, and dsDNA-Ab were also determined (Lkcxtech, Beijing, China; Shanghai Enzyme-linked Biotechnology Co., Ltd., Shanghai, China). The OD value was measured at 450 nm, and the concentrations were calculated based on the standard curve.

ScRNA-seq analysis

This study analyzed scRNA-seq data from the initial diagnosis stage of 9 patients with relapsed/refractory (R/R) AML previously conducted by our center [17]. Initially, data from all patients in the pre-treatment stage were selected, and $CD8^+$ T cells were extracted, yielding a total of 6,841 cells. Using the RStudio platform, $CD8^+$ T cells were divided into high-TIGAR expression and low-TIGAR expression groups based on the median expression value of TIGAR in these cells. Differential expression analysis was then conducted between these two groups to identify differentially expressed genes. Genes with a *P* value less than 0.05 and a Log2FC greater than 0.25 were considered upregulated in the high-TIGAR expression group. A volcano plot was generated to visualize the results, and a violin plot was used to illustrate the expression and distribution of the highly significant gene TIGAR between the high and low expression $CD8^+$ T cell groups. Subsequently, $CD8^+$ T cells with high TIGAR expression were selected and Gene Ontology (GO) pathway enrichment analysis of upregulated genes in this cell population was performed using the "clusterProfiler" package. Enriched pathways within the biological processes (BP), molecular functions (MF), and cellular components (CC) categories were compared and analyzed.

Single Sample Gene Set Enrichment Analysis (ssGSEA) is a single-sample extension method of Gene Set Enrichment Analysis (GSEA) that is suitable for scRNA-seq data. By matching gene expression values with specified gene sets, it calculates the activity score of a biological process or pathway in each sample, which can be implemented using the GSVA package in "R". We used ssGSEA to score the glycolysis gene set defined in the Kyoto Encyclopedia of Genes and Genomes (KEGG) metabolic pathway gene set file (details in Supplementary file 2) to assess the differences in glycolytic activity of $CD8^+$ T cells between high and low TIGAR expression groups. TCellSI [18] can score eight different states of T cells, and we calculated the TCellSI scores for the eight cell states of TIGAR high and low T cell groups from scRNA-seq data, comparing the two groups of cells in the progenitor exhaustion and terminal exhaustion states.

Statistical analysis

Continuous variables were presented as mean ± standard deviation (SD) for normally distributed data and as median (Interquartile Range, IQR) for non-normally distributed data. Unpaired or paired Student's t-tests were utilized for comparing two groups, while the Mann–Whitney U or Wilcoxon signed-rank tests were used for non-normally distributed data. Categorical variables were assessed using the Chi-square test or Fisher's exact test. ANOVA analysis was employed for group comparisons. Repeated measurements ANOVA examined changes in $CD4^+$ and $CD8^+$ T cell counts at various time points, with adjustments made for sphericity assumption violations using the Greenhouse–Geisser correction. Kaplan–Meier analysis and the log-rank test compared survival rates between groups. Statistical analyses were conducted using R software (version 4.2.2), SPSS 21.0 (IBM, USA), and graphs were generated using GraphPad Prism 9.0 (GraphPad Software, USA). All tests were two-sided, with statistical significance set at $P < 0.05$.

Results

TIGAR deficiency promotes the immune function of $CD8^+$ T cells from AML mice

First, we constructed TIGAR WT mice with AML and TIGAR KO mice with AML model. Then, through in vitro experiments, we hope to verify the impact of TIGAR knockout on the count and function of $CD4^+$ or $CD8^+$ T

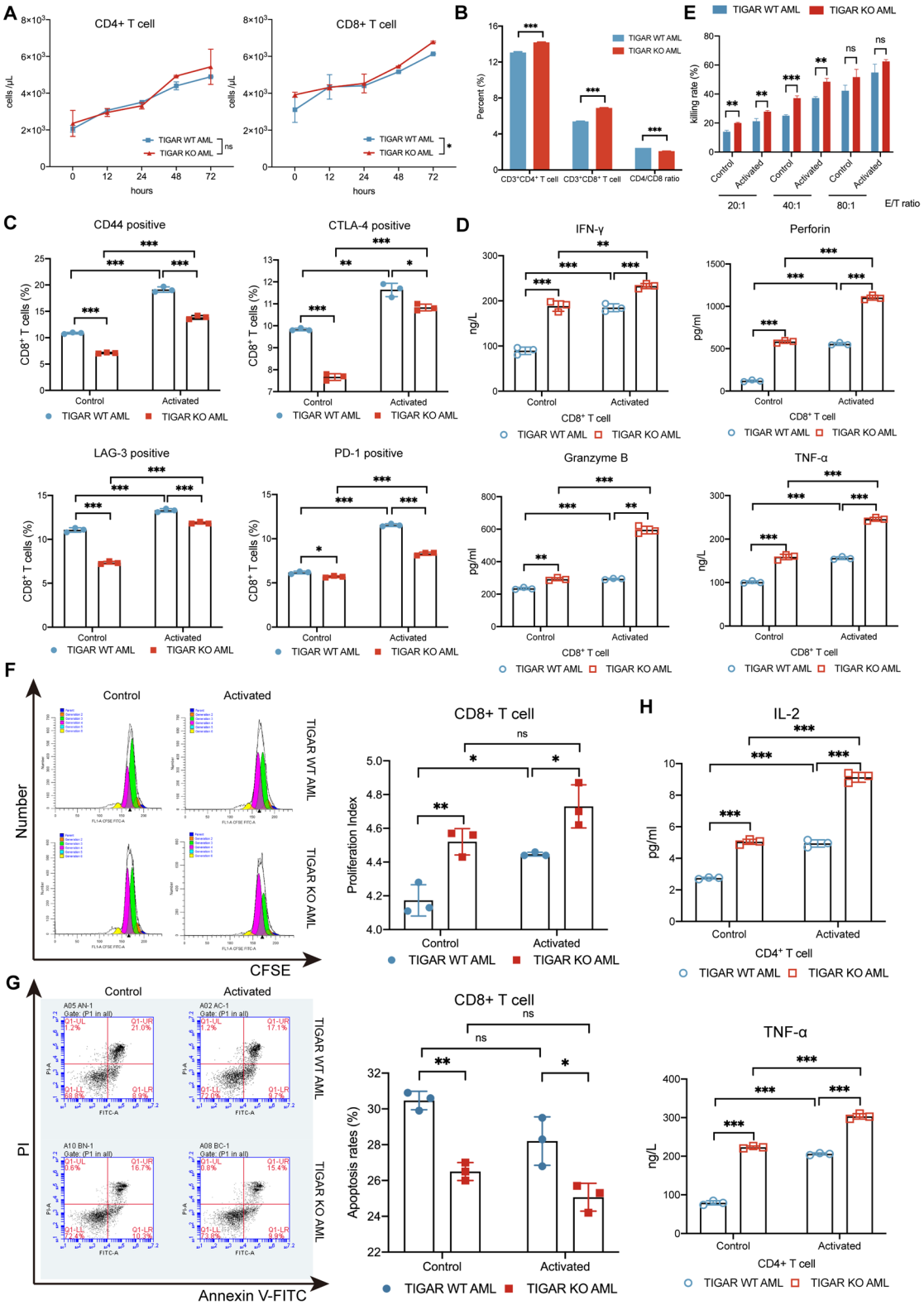

cells. The activation of splenic naïve $CD4^+$ T and $CD8^+$ T cells were induced by CD3/CD28 antibody, added to the medium containing IL-2 and continued to incubate for different times.

Flow cytometry was utilized to assess changes in cell counts at various time points—baseline (naïve), as well as 12 h, 24 h, 48 h, and 72 h post T-cell activation. Intriguingly, TIGAR deficiency increased $CD8^+$ T cell counts

◂**Fig. 1** TIGAR deficiency promotes the immune function of $CD8^+$ T cells from AML mice. **A** $CD4^+$ T (left) and $CD8^+$ T cell (right) count changes at baseline (naïve) and after induced activation from different mice. **B** The percentages of $CD3^+CD4^+$ and $CD3^+CD8^+$ T cells and the CD4/CD8 ratio from TIGAR WT and TIGAR KO mice with AML. **C** Cell surface expression of CD44, CTLA-4, LAG-3 and PD-1 on $CD8^+$ T cells. **D** IFN-γ, perforin, granzyme B, and TNF-α produced by $CD8^+$ T cells detected by ELISA. **E** The cytotoxicity of $CD8^+$ T cells towards AML cells (co-cultured at ratios of 20:1, 40:1, and 80:1). **F** Typical flow cytometry plot of CFSE staining (left) to identify proliferating $CD8^+$ T cells and proliferation index (right); Dark blue: Parent; Orange: Generation 2; Green: Generation 3; Purple: Generation 4; Light blue: Generation 5; Yellow: Generation 6. **G** Typical flow cytometry plot (left) and apoptosis rates (right) of $CD8^+$ T cells. **H** IL-2 (upper) and TNF-α (down) produced by $CD4^+$ T cells detected by ELISA. The values were presented as the mean ± SD of three independent experiments. *: $P<0.05$; **: $P<0.01$; ***: $P<0.001$; ns: not significant

in AML mice, with a non-significant rise in $CD4^+$ T cell count observed (Fig. 1A). Additionally, the CD4/CD8 ratio in AML mice (without activation) decreased upon TIGAR deletion (Fig. 1B). These findings may have implications for understanding the role of TIGAR in the context of AML immunology.

Next, we delved into the expression levels of molecules tied to cell surface activation and inhibition, encompassing CD44, crucial for T-cell migration and localization, and inhibitory markers like Cytotoxic T-lymphocyte-associated protein 4 (CTLA-4), Lymphocyte-activation gene 3 (LAG-3), and Programmed cell death protein 1 (PD-1). Post-activation, both TIGAR WT mice with AML and TIGAR KO mice with AML groups displayed a notable upsurge in these markers' expression (Fig. 1C). However, TIGAR deletion substantially diminished their expression, both at baseline and post-activation induction (Fig. 1C), hinting at TIGAR inhibition's potential to revive exhausted $CD8^+$ T cells and amplify their immune reactivity.

In TIGAR WT mice with AML and TIGAR KO mice with AML, activated $CD8^+$ T cells showcased a significant boost in intracellular IFN-γ, perforin, granzyme B, and TNF-α secretion (Fig. 1D). Remarkably, TIGAR ablation further intensified cytokine expression (Fig. 1D), suggesting TIGAR inhibition bolsters $CD8^+$ T cells' cytokine-secreting capacity in AML.

Furthermore, our study demonstrated that activated $CD8^+$ T cell cytotoxicity toward AML cells substantially increased post-activation, with TIGAR knockout notably enhancing killing efficiency at lower ratios but not higher ones (Fig. 1E). This enhancement appeared concentration-dependent rather than boundless.

The CFSE flow cytometry illustrated a substantial rise in $CD8^+$ T cell proliferation post-induced activation in TIGAR WT mice with AML, further escalated by TIGAR knockout (Fig. 1F, Table S1 in Supplementary file 3). The apoptosis rate of $CD8^+$ T cells revealed no change post-activation in TIGAR WT mice with AML but decreased significantly upon TIGAR deletion (Fig. 1G), indicating TIGAR inhibition fosters $CD8^+$ T cell proliferation and curtails apoptosis in AML.

Since TIGAR knockout minimally impacted $CD4^+$ T cell count, we explored its influence on cytokine secretion by these cells. Following induced activation, IL-2 and TNF-α production by $CD4^+$ T cells from TIGAR WT mice with AML surged significantly, further elevated by TIGAR inhibition (Fig. 1H).

TIGAR deficiency combined with glycolysis inhibitor prolongs the survival, reduces peripheral leukemia burden, and improves the infiltration of spleen in AML mice

Our previous study suggested that TIGAR is important for glycolysis of leukemia cells, and TIGAR knockdown sensitizes human leukemia cells to glycolysis inhibitor 2-DG [19] both in vitro and in *vivo* [8]. Therefore, TIGAR inhibitors combined with the glycolysis inhibitor 2-DG may be developed for the treatment of AML in the future. Although this study primarily investigates the effects of systemic knockout of TIGAR on T cells in AML mice, it also examines the impact of TIGAR knockout combined with 2-DG on the survival of AML mice, peripheral leukemia burden and the infiltration of leukemia in the liver and spleen, considering future drug development perspectives.

Here, we constructed 6 groups of mice, and observed their survival. We found that TIGAR WT mice with AML had significantly shorter survival compared to TIGAR WT or TIGAR KO normal control (4-week mortality: 80% vs. 0%, Fig. 2A, $P<0.05$). There is no statistically significant difference in OS between TIGAR KO and TIGAR WT mice with AML, but there is a trend towards extension. 2-DG-treated TIGAR KO mice with AML showed prolonged survival compared to TIGAR WT mice with AML (4-week mortality: 20% vs. 80%, Fig. 2A, $P<0.05$).

Flow cytometry analysis was utilized to detect the count of peripheral blood leukemia cells in different mouse models. The number of peripheral blood leukemia cells in TIGAR KO mice with AML was significantly lower than that in TIGAR WT mice with AML (Fig. 2B). In both TIGAR KO mice with AML and TIGAR WT mice with AML, treatment with 2-DG can reduce the number of peripheral blood leukemia cells (Fig. 2B). The combination of 2-DG and TIGAR KO in host had a synergistic effect (Fig. 2B).

The degree of leukemia infiltration in the liver and spleen at week 4 was assessed using H&E staining. In AML mice, both in the TIGAR WT background (AML proportion: 36.7% vs. 0%, $P<0.001$, Fig. 2, D) and in the TIGAR KO background (AML proportion: 26.7% vs. 0%, $P<0.001$,

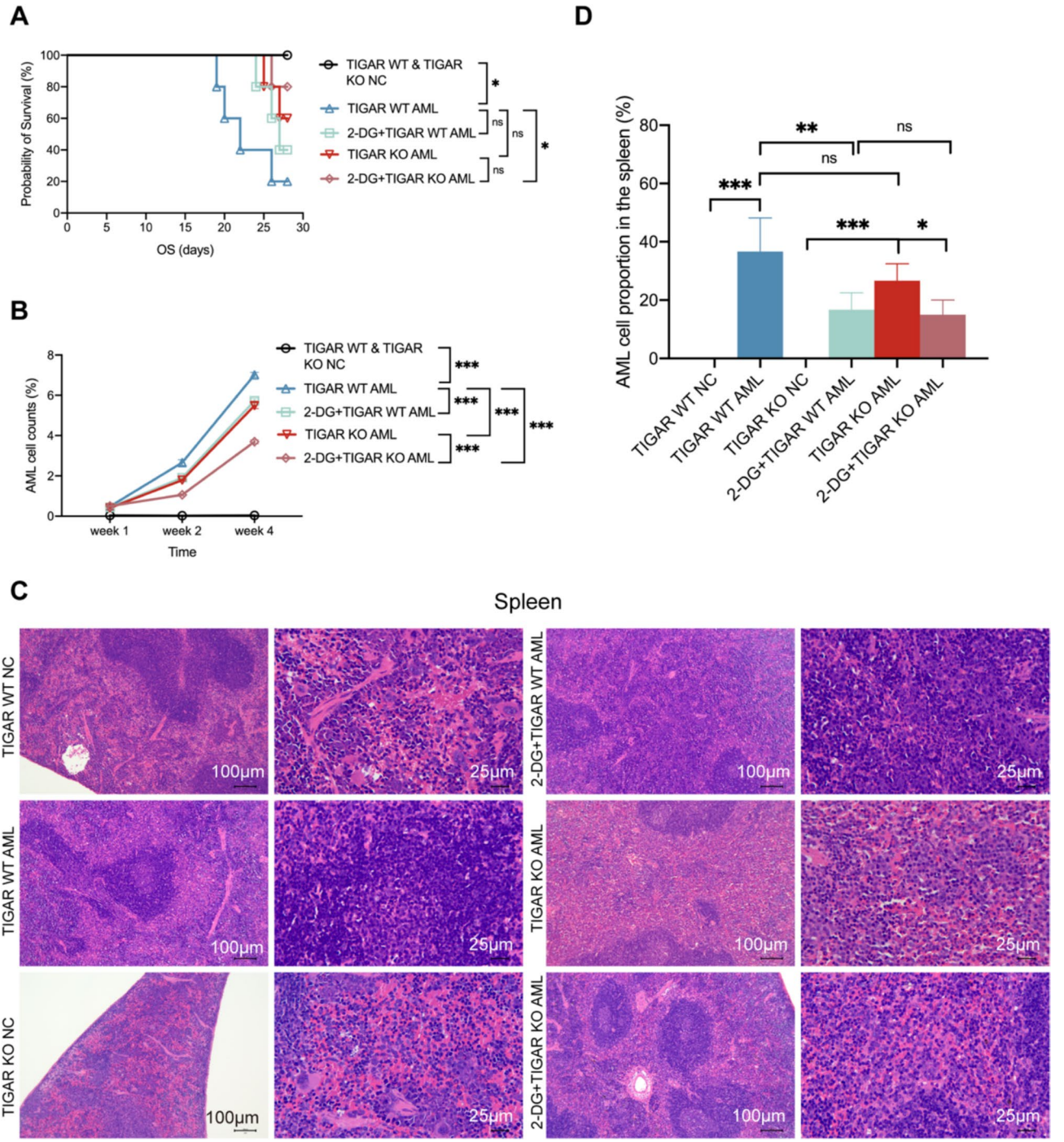

Fig. 2 TIGAR deficiency combined with glycolysis inhibitor prolongs the survival, reduces peripheral leukemia burden, and improves the infiltration of spleen in AML mice. **A** Survival of different mouse models (5 mice in each group). 2-DG-treated: mice were orally administered with a 2-DG solution at a dose of 2 g/kg, once daily for a total of 30 administrations, while other mice were orally administered an equal volume of saline solution. **B** Percentage of peripheral blood (from eyeballs) AML cells in different mouse models tested by flow cytometry (3 mice in each group at each time point). **C** Differences in leukemic cell infiltration in splenic tissues from different mouse models observed by H&E staining at 4 weeks of feeding (3 mice in each group). **D** The AML cell proportions in the spleens of different groups. The values were presented as the mean ± SD of independent experiments. *: $P < 0.05$; **: $P < 0.01$; ***: $P < 0.001$; ns: not significant

Fig. 2C, D), the degree of spleen infiltration was more severe than that in NC mice. Compared with TIGAR WT, TIGAR KO showed a decreasing trend in spleen infiltration in AML mice (AML proportion: 36.7% vs. 26.7%, $P=0.069$, Fig. 2C, D). After 2-DG treatment, in both TIGAR WT mice with AML (AML proportion: 16.7%, vs. 36.7%, $P=0.002$, Fig. 2C, D) and TIGAR KO mice with AML (AML proportion: 15% vs. 26.7%, $P=0.038$, Fig. 2C, D), the spleen infiltration of leukemia was significantly reduced compared with those without 2-DG treatment. In the 2-DG background, there was no statistically significant difference in spleen infiltration of AML with or without TIGAR KO (AML proportion: 15% vs. 16.7%, $P=0.745$, Fig. 2C, D). However, there was no significant liver leukemia infiltration in any of these six groups of mice (Fig. S1 in Supplementary file 3). This may be related to factors such as the number and cell viability of injected C1498 cells, the liver microenvironment of the host, and the anti-tumor immune ability.

The findings suggest that TIGAR knockout, combined with a glycolysis inhibitor, synergistically prolongs survival, reduces peripheral leukemia burden, and decreases the leukemic infiltration in spleen.

TIGAR deficiency restores thymic T cell development and peripheral T cell immune homeostasis in AML

The development and differentiation of T cells primarily occur in the thymus, where lymphoid progenitor cells mature and then distribute throughout the immune organs and tissues of the body via lymph and blood circulation to exert their immune functions. Within the thymus, T cells undergo a double negative (DN) and double positive (DP) stage. After undergoing positive and negative selection, they acquire MHC (major histocompatibility complex)-restricted development and become CD4 or CD8 single positive (SP) T cells. Immune homeostasis refers to the ability of the body's immune system to maintain its stable state in a dynamic balance. This balance includes effective resistance to foreign pathogens as well as adaptation and tolerance to self-tissues and harmless antigens in the environment. Immune homeostasis is one of the core functions of the immune system, ensuring the appropriateness and specificity of immune responses to avoid immune deficiencies or excessive reactions (such as inflammation or autoimmune diseases). Immune homeostasis depends on the dynamic balance between pro-inflammatory and anti-inflammatory cytokines. To further investigate the impact of TIGAR knockout on thymic T cell development and peripheral T cell immune homeostasis, we conducted the following in *vivo* mouse experiments. We constructed TIGAR WT NC, TIGAR WT mice with AML, and TIGAR KO mice with AML model, and then examined the development of thymic T cells (central immune organ), the proportions of naïve T, effector T, and memory T cells in the spleen (peripheral immune organ), as well as the expression of inflammatory factors in the mouse serum. In addition, we assessed the proliferation of splenic $CD4^+$ and $CD8^+$ T cells in the mice at different days using flow cytometry.

In TIGAR WT mice with AML, there was a significant increase in DN and $CD8^+$ SP cells, along with a decrease in DP cells in the thymus compared to normal controls (Fig. 3A). TIGAR knockout in mice with AML led to a notable increase in DP and $CD4^+$ SP cells and a decrease in $CD8^+$ SP cells in the thymus (Fig. 3A), indicating restoration of thymic T cell development disrupted by AML.

After isolating $CD4^+$ T or $CD8^+$ T cells using magnetic beads, the proportions of naïve T cells ($CD44^-CD62L^+$), effector T cells ($CD44^+CD62L^-$), and memory T cells ($CD44^+CD62L^+$) in splenic lymphocytes from different mouse models were determined using flow cytometry. Within $CD4^+$ and $CD8^+$ T cell subsets from spleen, TIGAR WT mice with AML exhibited decreased proportions of naïve and memory T cells and an increased proportion of effector T cells compared to normal controls (Fig. 3B). TIGAR knockout in mice with AML resulted in increased proportions of naïve and memory T cells and decreased effector T cells (Fig. 3B), suggesting restoration of peripheral T cell immune balance disrupted by AML.

In the realm of AML, the elevation of serum biomarkers such as IFN-γ, perforin, granzyme B, TNF-α, and dsDNA antibodies unveils profound immunological transformations, potentially heralding an increase in chronic inflammation and a disruption of immune homeostasis [20–23]. Our study found that TIGAR WT mice with AML displayed elevated levels of cytokines (IFN-γ, perforin, granzyme B, TNF-α) and dsDNA-Ab in serum compared to normal control, indicative of a pro-inflammatory state (Fig. 3C). However, TIGAR knockout in mice with AML reduced these inflammatory markers close to the normal range (Fig. 3C), suggesting a restoration of immune homeostasis.

Above results verified that TIGAR deficiency restores thymic T cell development and peripheral T cell immune homeostasis in AML.

To determine the effect of TIGAR knockout on the proliferation of peripheral T cells, we assessed the proliferation of splenic $CD4^+$ T and $CD8^+$ T cells at 7, 14, and 21 days after EDU injection using flow cytometry. There was no statistically significant difference in the proliferation of $CD4^+$ T cells at any time point between the TIGAR WT mice with AML and the normal control or between the TIGAR WT mice with AML and the TIGAR KO mice with AML (Fig. 4). The proliferation of $CD8^+$ T cells in TIGAR WT mice with AML significantly increased at day 7 and day 14 compared to normal controls (Fig. 5), highlighting a potential activation or expansion of $CD8^+$ T cells in response to the AML environment. TIGAR knockout significantly

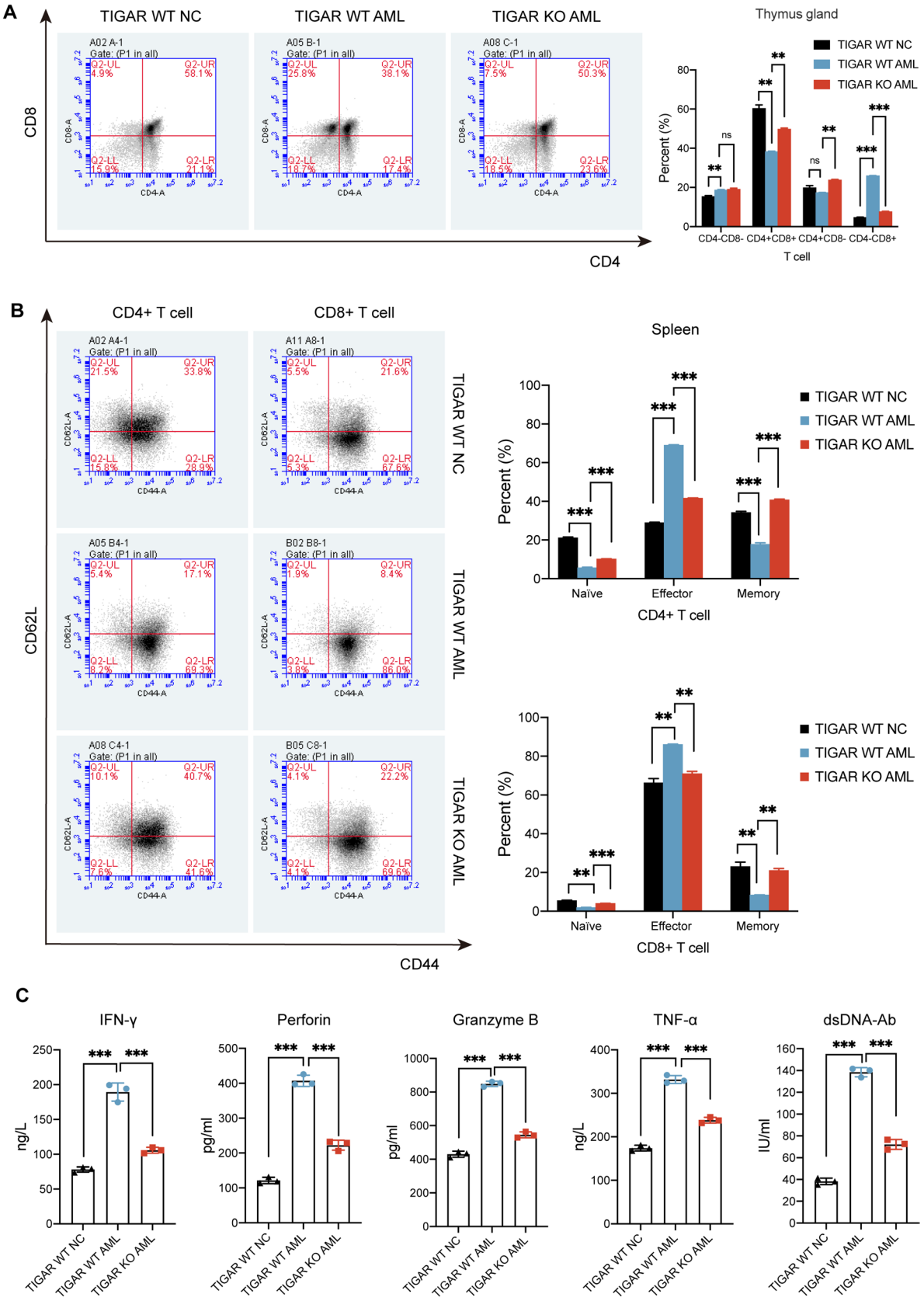
A
TIGAR WT NC
TIGAR WT AML
TIGAR KO AML
CD8
CD4
Thymus gland
TIGAR WT NC
TIGAR WT AML
TIGAR KO AML
Percent (%)
CD4-CD8- CD4+CD8+ CD4+CD8- CD4-CD8+
T cell
B
CD4+ T cell
CD8+ T cell
TIGAR WT NC
TIGAR WT AML
TIGAR KO AML
CD62L
CD44
Spleen
Naïve
Effector
Memory
CD4+ T cell
CD8+ T cell
C
IFN-γ
Perforin
Granzyme B
TNF-α
dsDNA-Ab
ng/L
pg/ml
IU/ml

◂**Fig. 3** Effect of TIGAR on thymic T cell development and peripheral T cell immune homeostasis. **A** Typical flow cytometry plot (left) and percentages of $CD4^-CD8^-$, $CD4^+CD8^+$, $CD4^+CD8^-$ and $CD4^-CD8^+$ T cells (right) in thymus glands from different mice. **B** Typical flow cytometry plot (left) and percentages of naïve, effector, and memory T cells in $CD4^+$ T (upper right) and $CD8^+$ T (lower right) cells of spleens from different mouse models. **C** IFN-γ, perforin, granzyme B, TNF-α, and dsDNA-Ab levels in serum of different mouse models. The values were presented as the mean ± SD of three independent experiments. **: $P < 0.01$; ***: $P < 0.001$; ns: not significant

reduced the proliferation of $CD8^+$ T cells at day 7 in AML mice, but there were no significant differences observed at other time points (Fig. 5). The lack of sustained differences in T cell proliferation post-TIGAR knockout may be attributed to compensatory mechanisms within the immune response, tumor microenvironmental suppressive signals, the transient nature of TIGAR's effects, and alterations in metabolic pathways linked to TIGAR's role in glucose metabolism. These factors could limit $CD8^+$ T cell proliferation despite the absence of TIGAR.

Biological functions of TIGAR in $CD8^+$ T cells based on scRNA-seq data analysis

To further clarify the biological functions of TIGAR in $CD8^+$ T cells, we reanalyzed scRNA-seq data from 9 AML patients in our center [17]. A total of 6,841 $CD8^+$ T cells were extracted and based on the median expression value of TIGAR in $CD8^+$ T cells, they were divided into high TIGAR expression and low TIGAR expression groups. The violin plot shows the expression of the TIGAR gene in $CD8^+$ T cells, with a significant expression in the high group and almost no expression in the low group (Fig. 6A). This may indicate that high expression of the TIGAR gene in $CD8^+$ T cells is associated with certain cellular functions or states. The volcano plot illustrates the differential expression of genes in the high and low TIGAR expression groups of $CD8^+$ T cells (Fig. 6B). It was found that the expression of genes such as LIME1, TRIAP1, CCNK, PTPRCAP, and BIN1 was significantly upregulated, while the expression of genes such as S100A8, LYZ, S100A9, ELANE, CD24, PRTN3, CAMP, and CEACAM8 was significantly downregulated. Subsequently, $CD8^+$ T cells with high TIGAR expression were selected and GO pathway enrichment analysis of upregulated genes in this cell population was performed (Fig. 6C, D). The results showed that in the BP category, the enriched significant entries were mainly focused on processes related to immune response, such as T cell receptor signaling pathway, antigen receptor-mediated signaling pathway, immune response-activating cell surface receptor signaling pathway, immune response-activating signal transduction, regulation of mRNA metabolic process, and T cell activation. In the MF category, the differential genes were significantly enriched in functions related to molecular binding and signal transduction, such as protein tyrosine kinase binding, receptor tyrosine kinase binding, and phosphatase binding. In the CC category, significant entries were concentrated in cellular structures such as nuclear speck, membrane region, membrane raft, membrane microdomain, and immunological synapse. These findings suggest that TIGAR plays a crucial role in modulating the immune responses of $CD8^+$ T cells in AML.

We further scored the expressions of glycolysis-related genes in $CD8^+$ T cells with high and low TIGAR expression groups by ssGSEA to evaluate the differences in glycolysis activity between the two groups of cells (Fig. 6E). We found that the score of glycolysis-related gene expressions in the TIGAR high-expression group was significantly higher than that in the TIGAR low-expression group, suggesting that TIGAR is involved in the glycolysis pathway, and high TIGAR expression may change gene expression patterns of the glycolysis pathway. Subsequently, we used TCellSI to score the progenitor exhaustion and terminal exhaustion states of the two groups and found that both the progenitor exhaustion and terminal exhaustion scores in the TIGAR high-expression group were significantly higher than those in the TIGAR low-expression group (Fig. 6F). In addition, the average expression levels of exhaustion-related markers in the TIGAR high-expression group: PD-1, LAG-3, T cell immunoglobulin and mucin domain-containing protein 3 (TIM-3), CTLA-4 and T cell immunoglobulin and ITIM domain (TIGIT) were all significantly higher than those in the TIGAR low-expression group (Fig. 6G). The above results further confirmed that the high expression of TIGAR may be related to the exhaustion of $CD8^+$ T cells, and TIGAR KO may restore the exhausted state of $CD8^+$ T cells, thereby improving the prognosis of AML.

Discussion

Understanding the immune microenvironment in AML is of paramount importance, as it plays a critical role in tumor progression and patient prognosis. AML is characterized by the rapid proliferation of myeloid progenitor cells, leading to impaired hematopoiesis and immune dysfunction [24, 25]. Recent studies have highlighted an immunosuppressive milieu in blood and bone marrow samples of AML patients, characterized by increased regulatory T cells (Tregs) and myeloid-derived suppressor cells (MDSCs), reduced T cell proliferation, elevated immune checkpoint molecules, and a rise in terminally exhausted T cells [26–31]. AML cells and the bone marrow microenvironment contribute to T cell suppression via cytokine release and inhibitory molecules. For instance, AML cells activate PD-1 signaling through Programmed death-ligand

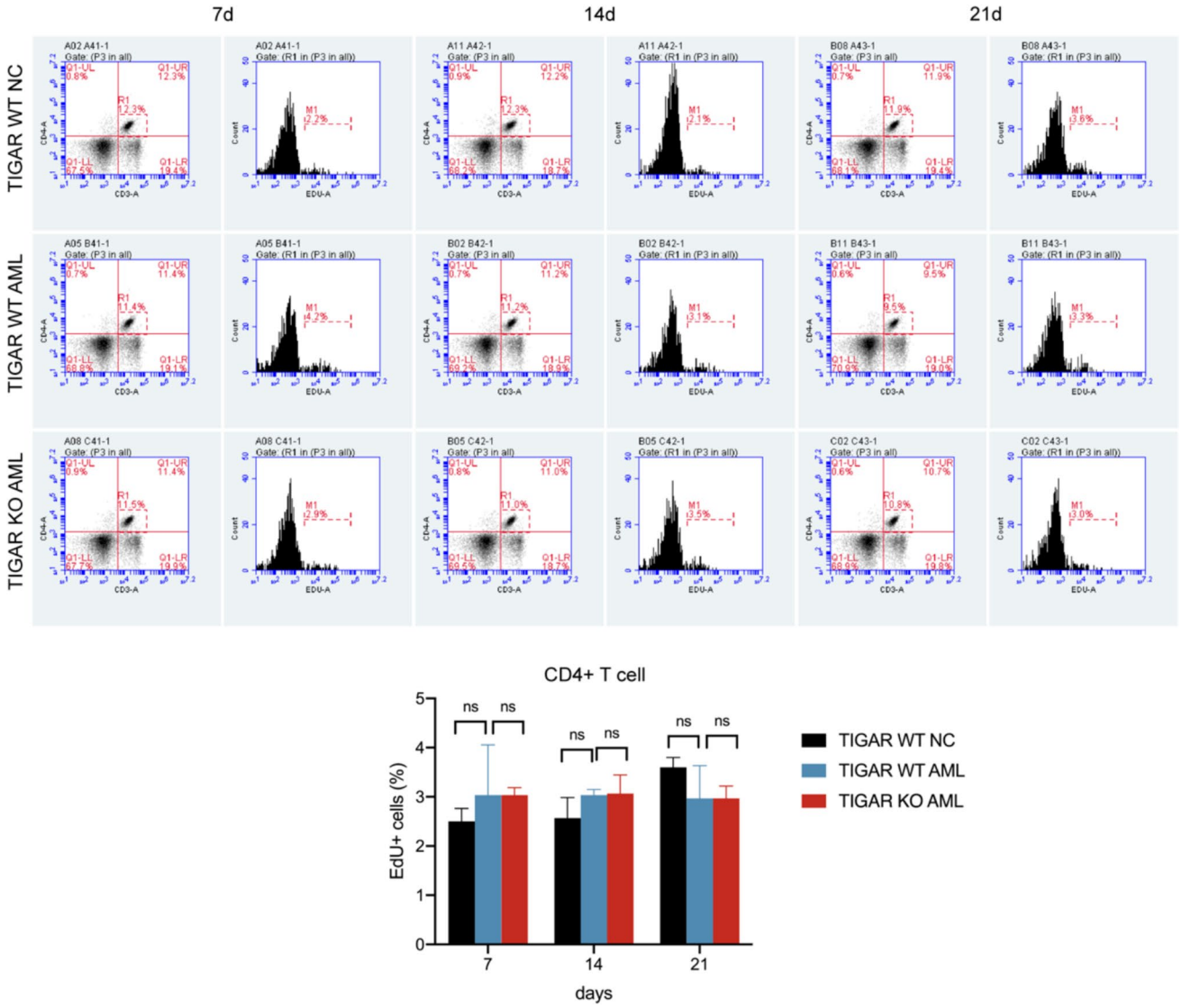

Fig. 4 Effect of TIGAR on proliferation of in vivo $CD4^+$ T cells in AML mice. Typical flow cytometry plot (upper) and proliferation of $CD4^+$ T cells (down) in the spleen lymphocytes of TIGAR WT mice with AML, TIGAR KO mice with AML and normal control at 7, 14, and 21 days after EDU injection. The values were presented as the mean ± SD of three independent experiments. ns: not significant

1 (PD-L1) expression, while macrophages and dendritic cells express PD-L2, inhibiting T cell function [32]. Thymic atrophy in AML leads to decreased peripheral T cells, increased Tregs, and memory T cell subsets, limiting immune responses against AML cells [33–35]. Dysfunctional $CD8^+$ T cells in AML patients exhibit abnormal phenotypes and upregulated exhaustion markers, impairing cytotoxicity against AML cells [25, 31, 36]. The altered T lymphocyte function and count in AML patients, influenced by inflammatory changes, impact immune responses and clinical outcomes [24, 37]. Our study in AML mice aligns with these findings, demonstrating disrupted T cell immunity in central and peripheral immune organs.

This study focuses on the role of TIGAR in modulating the immune response of $CD8^+$ T cells within the context of AML. We hypothesize that TIGAR influences T cell activation, proliferation, and cytokine production, ultimately shaping the immune landscape of AML. Our findings demonstrate that TIGAR deficiency enhances $CD8^+$ T cell functions, reduces exhaustion markers, and improves overall immune responses against AML cells. This study not only elucidates the molecular mechanisms underpinning T cell exhaustion in AML but also suggests that targeting TIGAR could serve as a therapeutic strategy to restore effective anti-tumor immunity.

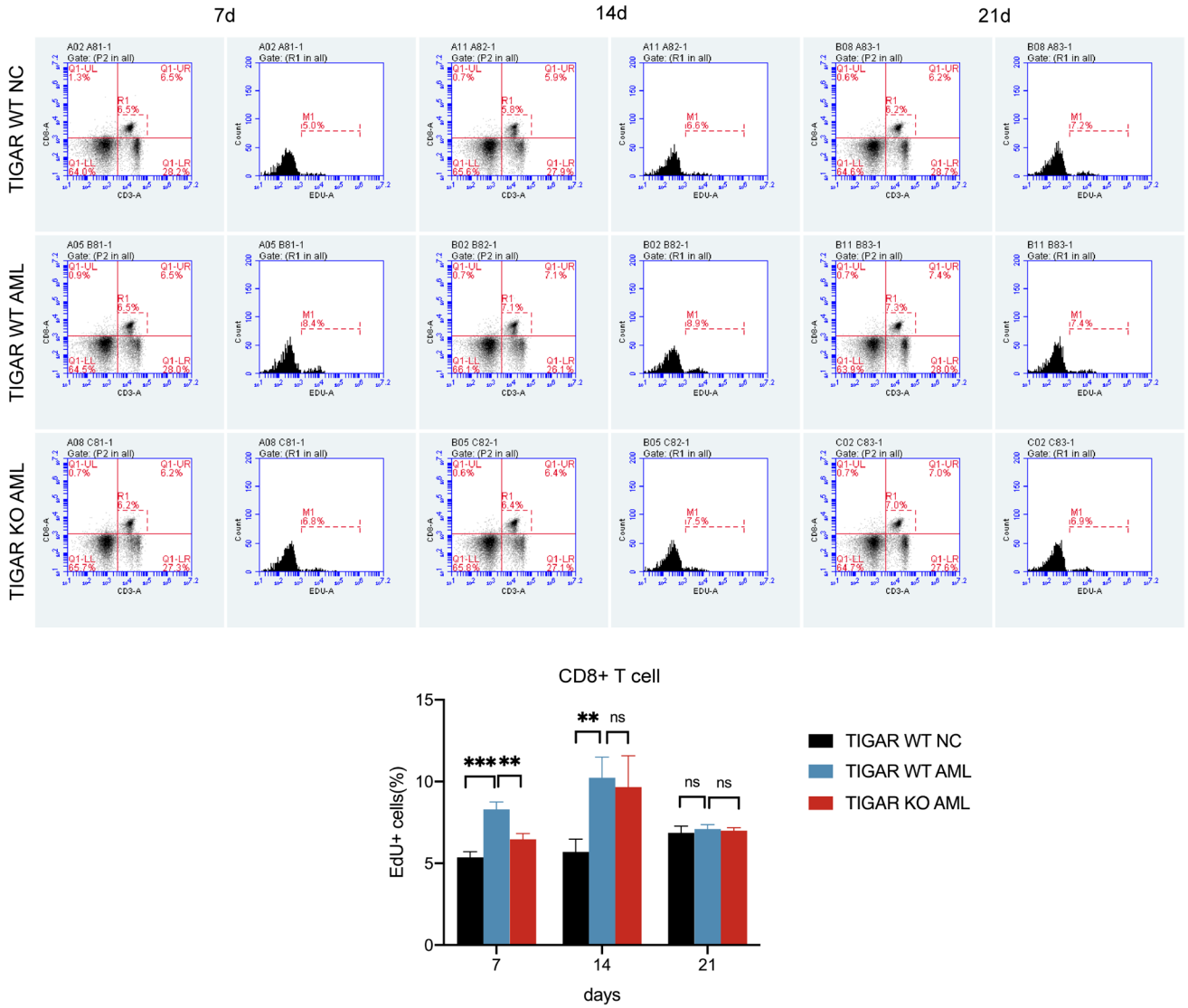

Fig. 5 Effect of TIGAR on proliferation of in vivo $CD8^+$ T cells in AML mice. Typical flow cytometry plot (upper) and proliferation of $CD8^+$ T cells (down) in the spleen lymphocytes of TIGAR WT mice with AML, TIGAR KO mice with AML and normal control at 7, 14, and 21 days after EDU injection. The values were presented as the mean ± SD of three independent experiments. **: $P < 0.01$; ***: $P < 0.001$; ns: not significant

The results of this study significantly enhance our understanding of the molecular mechanisms by which TIGAR influences $CD8^+$ T cell function in AML. Our findings indicate that TIGAR plays a crucial role in modulating T cell activation, proliferation, and cytokine production, thereby contributing to the overall immune response. Specifically, TIGAR deficiency was associated with increased production of key effector cytokines such as IFN-γ, perforin, granzyme B, and TNF-α, which are vital for T cell-mediated cytotoxicity against AML cells. This suggests that TIGAR may act as a metabolic checkpoint that limits T cell functionality, thereby promoting immune evasion in AML. Targeting TIGAR could, therefore, represent a novel therapeutic strategy to enhance anti-tumor immunity by overcoming the metabolic barriers that suppress T cell responses in the tumor microenvironment [38].

Furthermore, the observed reduction in apoptosis rates and increased proliferation of $CD8^+$ T cells upon TIGAR knockout underscores the importance of metabolic regulation in T cell survival and expansion within the tumor microenvironment. The interplay between cellular metabolism and immune function is increasingly recognized as a critical determinant in cancer progression and treatment outcomes. By elucidating the impact of TIGAR on metabolic pathways, particularly glycolysis, this study provides valuable insights into the potential for combining metabolic inhibitors

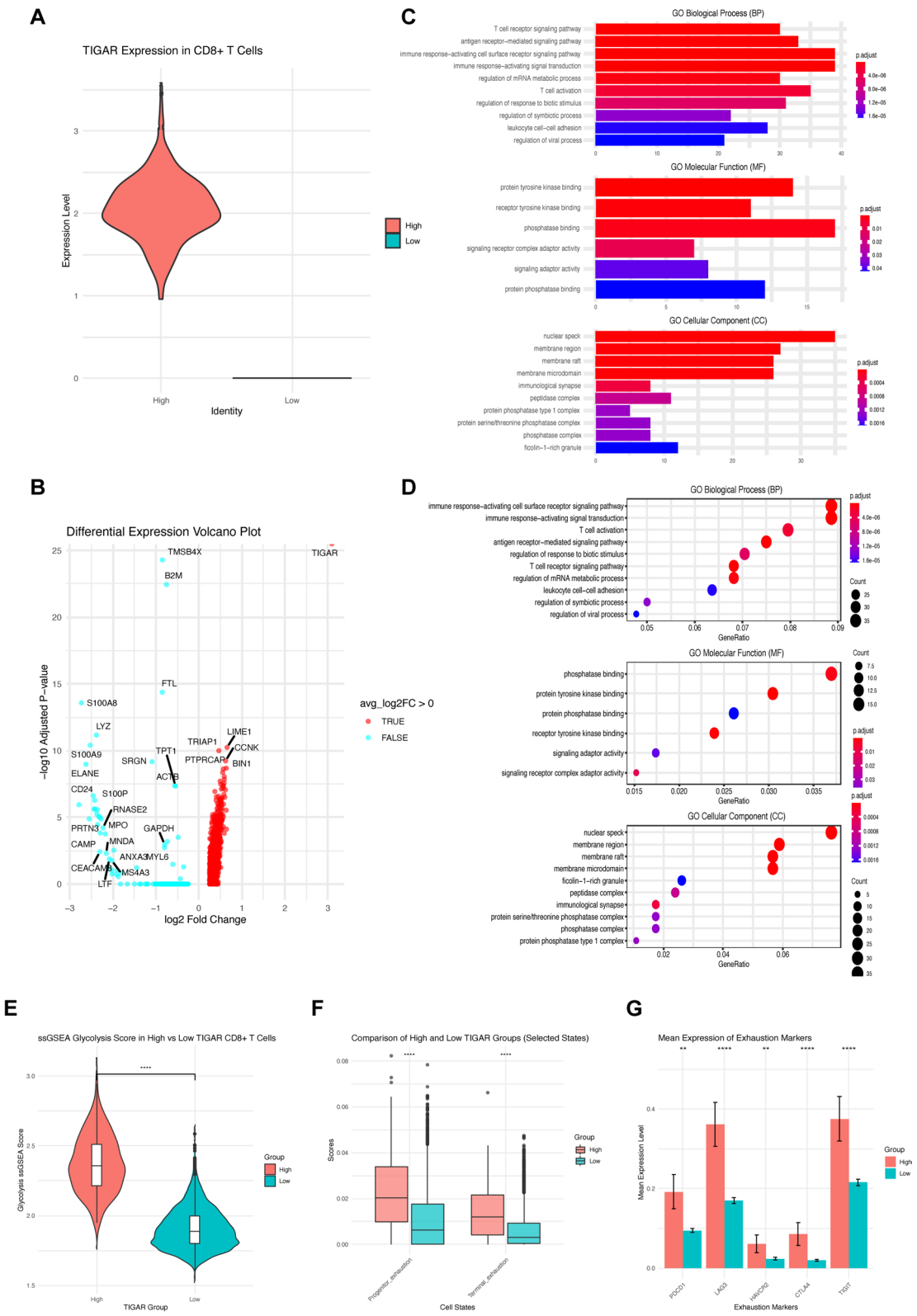

with immunotherapies. Such combination approaches could exploit the metabolic vulnerabilities of AML cells while simultaneously restoring T cell function, thereby enhancing therapeutic efficacy.

◂**Fig. 6** Biological function of TIGAR in $CD8^+$ T cells based on scRNA-seq data analysis. **A** The violin plot shows the expression of the TIGAR gene in $CD8^+$ T cells, with the x-axis representing cells from high/low TIGAR expression groups and the y-axis indicating the gene expression level of the TIGAR gene. The shape of the violin plot reflects the distribution of TIGAR expression levels in the high expression group, with the width indicating the density of samples at different expression levels. **B** Volcano plot of differentially expressed genes in $CD8^+$ T cells with high and low expression of TIGAR. The x-axis (log2 Fold Change) represents the fold change in gene expression, with larger values indicating greater upregulation and smaller (negative) values indicating greater downregulation. The y-axis (-log10 Adjusted *P* value) represents the negative logarithmic transformation of the *P* value, with higher values indicating stronger statistical significance of gene differential expression. Points are color-coded in the plot: red points (TRUE) indicate upregulated genes, while blue points (FALSE) indicate downregulated genes. Bar plot (**C**) and bubble plot (**D**) formats of the Gene Ontology (GO) analysis. The bar plot summarizes the significant biological processes (BP), molecular functions (MF), and cellular components (CC). The bar plot displays the number of enriched genes on the x-axis and the enriched GO terms on the y-axis. Red indicates highly significant terms with adjusted *P* values (p.adjust < 0.001), while shades of blue and purple represent decreasing significance. The bubble plot provides a visual representation of the GO analysis results, displaying significant BP, MF, and CC in relation to gene ratio and adjusted *P* values. The x-axis representing the Gene Ratio, which is the ratio of enriched genes to the total number of genes for each GO term, while the y-axis shows the adjusted *P* values. The size of the bubbles indicates the count of associated genes, with larger bubbles representing a higher count. The analysis of **C** and **D** is based on the upregulated genes enriched in the TIGAR high expression group of $CD8^+$ T cells. **E** The comparison of glycolysis scores between the high and low expression groups of TIGAR in $CD8^+$ T cells. The x-axis represents the high (red) and low (green) expression groups of TIGAR, while the y-axis represents the glycolysis scores, reflecting the overall activity of glycolysis-related genes. **F** The comparison of TIGAR high (red) and low (green) expression groups under different states. The x-axis represents the different states of $CD8^+$ T cells, specifically the progenitor exhaustion and terminal exhaustion states, while the y-axis indicates the corresponding scores. **G** The average expression levels of exhaustion-related markers in the TIGAR high (red) and low (green) expression groups. The x-axis indicates different markers, while the y-axis shows the average expression levels, with error bars representing the standard error. PDCD1: PD-1; LAG3: LAG-3; HAVCR2: TIM-3; CTLA4: CTLA-4. **: $P < 0.01$; ****: $P < 0.0001$

In terms of immune mechanisms, this study highlights the relationship between TIGAR expression and markers of T cell exhaustion, such as PD-1, LAG-3, TIM-3, CTLA-4 and TIGIT. The correlation between high TIGAR levels and increased expression of exhaustion markers suggests that TIGAR may play a role in mediating immune suppression in the tumor microenvironment. Naïve T cells typically rely on OXPHOS for energy needs, but activation through T cell receptor (TCR) and CD28 co-stimulation triggers aerobic glycolysis via mTOR [39], facilitating clonal expansion and effector functions like IFN-γ production [11, 40]. Glucose deprivation impairs downstream TCR signaling, proliferation, and cytokine production, resulting in an exhausted-like state [41, 42]. TIGAR inhibits glycolysis [13], while activated and proliferating T cells require glycolysis. Therefore, high expression of TIGAR may inhibit T cell activity by suppressing glycolysis, causing T cells to enter an exhausted state. This explains the possible mechanism by which inhibiting TIGAR can restore the exhausted state of T cells. Understanding these mechanisms is essential for developing innovative immunotherapeutic strategies that not only target the tumor cells but also reinvigorate exhausted T cell populations. This work lays the groundwork for future research aimed at leveraging TIGAR as a therapeutic target in combination with immune checkpoint inhibitors, which may enhance clinical outcomes for AML patients [43].

In this study, a seemingly paradoxical situation was encountered and can be explained as follows. The glycolysis-related gene expression score in the TIGAR high-expression group was much higher than in the low-expression group, seemingly indicating a positive relation between TIGAR and these genes. However, it's just a correlative finding. In specific situations, TIGAR may have a complex regulatory link with these genes. High TIGAR expression may change gene expression patterns but not necessarily promote glycolytic function. As we know, TIGAR inhibits glycolysis, and activated and proliferating T cells rely on glycolysis for energy. So, high TIGAR expression may impede T-cell activity by suppressing glycolysis. Overall, there's no real contradiction. Mechanistically, despite the complex connection between TIGAR and glycolysis-related gene expressions, TIGAR inhibits glycolysis. In T cells, as they get energy via glycolytic metabolism, this inhibition restricts T-cell activity. Comprehending these relationships needs considering both gene-expression-level regulatory interactions and functional impacts on cellular activities like in T cells.

This study's significance lies in revealing that TIGAR KO mice with AML restores T cell activity, alleviates T cell exhaustion, reestablishes immune balance, thereby reducing tumor load and enhancing OS in AML. The mechanism might involve changes in energy metabolism of T cells because of the key role of TIGAR in glycolysis. Furthermore, this work introduced a TIGAR KO mouse model, validating TIGAR's impact on AML prognosis and T cell immunity through diverse in vitro and in vivo methods. The primary limitation is its reliance solely on animal studies and scRNA-seq data without human cell line validation. Besides, since 2-DG treatment was initiated on day 1, presumably before leukemia engraftment, it is possible that 2-DG may interfere with leukemia cell engraftment. 2-DG can disrupt glucose availability and related metabolites needed for leukemia cells' initial survival and colonization. Also, it may modulate the interactions between leukemia cells and host cells during engraftment, affecting immune recognition or evasion. The anti-leukemia activity in established models mainly involves disrupting abnormal metabolism, inducing apoptosis, and inhibiting proliferation. But the potential

interference with engraftment is an extra factor. Future studies should start 2-DG treatment at different time points relative to leukemia cell injection to better understand its role in different leukemia development stages in TIGAR WT and TIGAR KO AML mouse models.

AML is a heterogeneous hematological malignancy marked by immune suppression and T-cell dysfunction. Using a TIGAR knockout mice with AML model, we observed that silencing TIGAR boosts $CD8^+$ T cell proliferation, enhances function, alleviates immune fatigue, triggers anti-leukemic effects, and rebalances peripheral immunity. These findings underpin future anti-AML strategies.

Supplementary Information The online version contains supplementary material available at https://doi.org/10.1007/s00262-025-04042-y.

Acknowledgements We would like to express our gratitude to Nanjing Medical University for providing the experimental venue and facilities.

Author contributions QS and SQ designed the study; JC, WL, YF and PX done the mice experiments; SZ, XH, WZ and KL done the single-cell RNA sequencing analysis; CX and RW done the H&E staining and related pathology experiments; MH and QS analyzed and interpreted the data; JC, WL and SZ drafted the manuscript; QS and SQ revised and supervised the manuscript. All authors have read and approved the manuscript.

Funding This work was supported by the National Natural Science Foundation of China under Grant 82170153 and 81870119; Young Scholars Fostering Fund of the First Affiliated Hospital of Nanjing Medical University under Grant PY2023025; Jiangsu Province Hospital (the First Affiliated Hospital with Nanjing Medical University) Clinical Capacity Enhancement Project under Grant JSPH-MC-2023-11; and Medical Innovation Team under Grant CXZX202222.

Data availability The datasets generated during and/or analysed during the current study are available from the corresponding author on reasonable request.

Declarations

Conflict of interest The authors declare no competing interests.

Ethical approval The animal care and laboratory procedures were approved by the Ethics Committee of the First Affiliated Hospital of Nanjing Medical University, Jiangsu Province Hospital (approval number: 2018-SRFA-132).

References

1. Panuzzo C, Jovanovski A, Ali MS et al (2022) Revealing the mysteries of acute myeloid leukemia: from quantitative PCR through next-generation sequencing and systemic metabolomic profiling. J Clin Med 11(3):483. https://doi.org/10.3390/jcm11030483
2. Hanahan D, Weinberg RA (2011) Hallmarks of cancer: the next generation. Cell 144(5):646–674. https://doi.org/10.1016/j.cell.2011.02.013
3. Eason K, Sadanandam A (2016) Molecular or metabolic reprograming: what triggers tumor subtypes? Cancer Res 76(18):5195–5200. https://doi.org/10.1158/0008-5472.CAN-16-0141
4. Warburg O (1956) On the origin of cancer cells. Science 123(3191):309–314. https://doi.org/10.1126/science.123.3191.309
5. Kozal K, Jozwiak P, Krzeslak A (2021) Contemporary perspectives on the Warburg effect inhibition in cancer therapy. Cancer Control 28:10732748211041244. https://doi.org/10.1177/10732748211041243
6. Joshi SK, Nechiporuk T, Bottomly D et al (2021) The AML microenvironment catalyzes a stepwise evolution to gilteritinib resistance. Cancer Cell 39(7):999-1014 e8. https://doi.org/10.1016/j.ccell.2021.06.003
7. Saito Y, Sawa D, Kinoshita M et al (2020) EVI1 triggers metabolic reprogramming associated with leukemogenesis and increases sensitivity to L-asparaginase. Haematologica 105(8):2118–2129. https://doi.org/10.3324/haematol.2019.225953
8. Qian S, Li J, Hong M et al (2016) TIGAR cooperated with glycolysis to inhibit the apoptosis of leukemia cells and associated with poor prognosis in patients with cytogenetically normal acute myeloid leukemia. J Hematol Oncol 9(1):128. https://doi.org/10.1186/s13045-016-0360-4
9. Hong M, Zhu Y, Zhao HH et al (2017) Overexpression of TIGAR predicts poor prognosis in elderly patients with cytogenetically normal acute myeloid leukemia (CN-AML). Int J Clin Exp Pathol 10(4):4748–4755
10. Zhang L, Romero P (2018) Metabolic control of CD8(+) T cell fate decisions and antitumor immunity. Trends Mol Med 24(1):30–48. https://doi.org/10.1016/j.molmed.2017.11.005
11. Menk AV, Scharping NE, Moreci RS et al (2018) Early TCR signaling induces rapid aerobic glycolysis enabling distinct acute T cell effector functions. Cell Rep 22(6):1509–1521. https://doi.org/10.1016/j.celrep.2018.01.040
12. Chang CH, Qiu J, O'Sullivan D et al (2015) Metabolic competition in the tumor microenvironment is a driver of cancer progression. Cell 162(6):1229–1241. https://doi.org/10.1016/j.cell.2015.08.016
13. Tang J, Chen L, Qin ZH, Sheng R (2021) Structure, regulation, and biological functions of TIGAR and its role in diseases. Acta Pharmacol Sin 42(10):1547–1555. https://doi.org/10.1038/s41401-020-00588-y
14. Li X, Wu L, Zopp M, Kopelov S, Du W (2019) p53-TP53-induced glycolysis regulator mediated glycolytic suppression attenuates DNA damage and genomic instability in fanconi anemia hematopoietic stem cells. Stem Cells 37(7):937–947. https://doi.org/10.1002/stem.3015
15. Wang H, Cheng Q, Li X et al (2018) Loss of TIGAR induces oxidative stress and meiotic defects in oocytes from obese mice. Mol Cell Proteomics 17(7):1354–1364. https://doi.org/10.1074/mcp.RA118.000620
16. Hong M, Xia Y, Zhu Y et al (2016) TP53-induced glycolysis and apoptosis regulator protects from spontaneous apoptosis and predicts poor prognosis in chronic lymphocytic leukemia. Leuk Res 50:72–77. https://doi.org/10.1016/j.leukres.2016.09.013

17. Li K, Du Y, Cai Y et al (2023) Single-cell analysis reveals the chemotherapy-induced cellular reprogramming and novel therapeutic targets in relapsed/refractory acute myeloid leukemia. Leukemia 37(2):308–325. https://doi.org/10.1038/s41375-022-01789-6
18. Yang JM, Zhang N, Luo T et al (2024) TCellSI: a novel method for T cell state assessment and its applications in immune environment prediction. Imeta 3(5):e231. https://doi.org/10.1002/imt2.231
19. Singh R, Gupta V, Kumar A, Singh K (2023) 2-deoxy-D-glucose: a novel pharmacological agent for killing hypoxic tumor cells, oxygen dependence-lowering in covid-19, and other pharmacological activities. Adv Pharmacol Pharm Sci 2023:9993386. https://doi.org/10.1155/2023/9993386
20. Xie X, Zhang W, Zhou X et al (2023) Low doses of IFN-γ maintain self-renewal of leukemia stem cells in acute myeloid leukemia. Oncogene 42(50):3657–3669. https://doi.org/10.1038/s41388-023-02874-5
21. Voskoboinik I, Whisstock JC, Trapani JA (2015) Perforin and granzymes: function, dysfunction and human pathology. Nat Rev Immunol 15(6):388–400. https://doi.org/10.1038/nri3839
22. Sanchez-Correa B, Bergua JM, Campos C et al (2013) Cytokine profiles in acute myeloid leukemia patients at diagnosis: survival is inversely correlated with IL-6 and directly correlated with IL-10 levels. Cytokine 61(3):885–91. https://doi.org/10.1016/j.cyto.2012.12.023
23. Fujii H, Cuvelier G, She K et al (2008) Biomarkers in newly diagnosed pediatric-extensive chronic graft-versus-host disease: a report from the Children's Oncology Group. Blood 111(6):3276–85. https://doi.org/10.1182/blood-2007-08-106286
24. Rutella S, Vadakekolathu J, Mazziotta F et al (2022) Immune dysfunction signatures predict outcomes and define checkpoint blockade-unresponsive microenvironments in acute myeloid leukemia. J Clin Invest 132(21):e159579. https://doi.org/10.1172/JCI159579
25. Tan J, Yu Z, Huang J et al (2020) Increased PD-1+Tim-3+ exhausted T cells in bone marrow may influence the clinical outcome of patients with AML. Biomark Res 8:6. https://doi.org/10.1186/s40364-020-0185-8
26. Wan Y, Zhang C, Xu Y et al (2020) Hyperfunction of CD4 CD25 regulatory T cells in de novo acute myeloid leukemia. BMC Cancer 20(1):472. https://doi.org/10.1186/s12885-020-06961-8
27. Wang L, Jia B, Claxton DF et al (2018) VISTA is highly expressed on MDSCs and mediates an inhibition of T cell response in patients with AML. Oncoimmunology 7(9):e1469594. https://doi.org/10.1080/2162402X.2018.1469594
28. Lamble AJ, Kosaka Y, Laderas T et al (2020) Reversible suppression of T cell function in the bone marrow microenvironment of acute myeloid leukemia. Proc Natl Acad Sci U S A 117(25):14331–14341. https://doi.org/10.1073/pnas.1916206117
29. Williams P, Basu S, Garcia-Manero G et al (2019) The distribution of T-cell subsets and the expression of immune checkpoint receptors and ligands in patients with newly diagnosed and relapsed acute myeloid leukemia. Cancer 125(9):1470–1481. https://doi.org/10.1002/cncr.31896
30. Noviello M, Manfredi F, Ruggiero E et al (2019) Bone marrow central memory and memory stem T-cell exhaustion in AML patients relapsing after HSCT. Nat Commun 10(1):1065. https://doi.org/10.1038/s41467-019-08871-1
31. Romine KA, MacPherson K, Cho HJ et al (2023) BET inhibitors rescue anti-PD1 resistance by enhancing TCF7 accessibility in leukemia-derived terminally exhausted CD8(+) T cells. Leukemia 37(3):580–592. https://doi.org/10.1038/s41375-023-01808-0
32. Yang X, Ma L, Zhang X, Huang L, Wei J (2022) Targeting PD-1/PD-L1 pathway in myelodysplastic syndromes and acute myeloid leukemia. Exp Hematol Oncol 11(1):11. https://doi.org/10.1186/s40164-022-00263-4
33. Li Y, Yin Q, Yang L et al (2009) Reduced levels of recent thymic emigrants in acute myeloid leukemia patients. Cancer Immunol Immunother 58(7):1047–1055. https://doi.org/10.1007/s00262-008-0621-3
34. Driss V, Quesnel B, Brinster C (2015) Monocyte chemoattractant protein 1 (MCP-1/CCL2) contributes to thymus atrophy in acute myeloid leukemia. Eur J Immunol 45(2):396–406. https://doi.org/10.1002/eji.201444736
35. Ustun C, Miller JS, Munn DH, Weisdorf DJ, Blazar BR (2011) Regulatory T cells in acute myelogenous leukemia: is it time for immunomodulation? Blood 118(19):5084–5095. https://doi.org/10.1182/blood-2011-07-365817
36. Wang M, Bu J, Zhou M et al (2018) CD8(+)T cells expressing both PD-1 and TIGIT but not CD226 are dysfunctional in acute myeloid leukemia (AML) patients. Clin Immunol 190:64–73. https://doi.org/10.1016/j.clim.2017.08.021
37. Lasry A, Nadorp B, Fornerod M et al (2023) An inflammatory state remodels the immune microenvironment and improves risk stratification in acute myeloid leukemia. Nat Cancer 4(1):27–42. https://doi.org/10.1038/s43018-022-00480-0
38. Liu Z, Wu Y, Zhang Y et al (2019) TIGAR promotes tumorigenesis and protects tumor cells from oxidative and metabolic stresses in gastric cancer. Front Oncol 9:1258. https://doi.org/10.3389/fonc.2019.01258
39. Shi LZ, Wang R, Huang G et al (2011) HIF1alpha-dependent glycolytic pathway orchestrates a metabolic checkpoint for the differentiation of TH17 and Treg cells. J Exp Med 208(7):1367–1376. https://doi.org/10.1084/jem.20110278
40. Chang CH, Curtis JD, Maggi LB Jr et al (2013) Posttranscriptional control of T cell effector function by aerobic glycolysis. Cell 153(6):1239–1251. https://doi.org/10.1016/j.cell.2013.05.016
41. Cham CM, Driessens G, O'Keefe JP, Gajewski TF (2008) Glucose deprivation inhibits multiple key gene expression events and effector functions in CD8+ T cells. Eur J Immunol 38(9):2438–2450. https://doi.org/10.1002/eji.200838289
42. Cham CM, Gajewski TF (2005) Glucose availability regulates IFN-gamma production and p70S6 kinase activation in CD8+ effector T cells. J Immunol 174(8):4670–4677. https://doi.org/10.4049/jimmunol.174.8.4670
43. Agudo J, Miao Y (2025) Stemness in solid malignancies: coping with immune attack. Nat Rev Cancer 25(1):27–40. https://doi.org/10.1038/s41568-024-00760-0